Applied trajectory generation to dock a feeder vessel

Bas. J. de Kruif

MARIN, Maritime Research Institute Netherlands, Wageningen
(e-mail: b.j.d.kruif@marin.nl)

Abstract: Autonomous sailing is seen as one of the possible solutions to cope with the decrease in qualified officers, to minimise the risk to humans and ships at challenging conditions, and to decrease the environmental impact of the transport sector. Autonomous sailing is not limited to moving the vessel safely through the seas, but it also includes docking the vessel. Docking is considered a difficult and critical manoeuvre in autonomous sailing.
The objective of this work is to construct a trajectory including its time derivatives for our newly designed 71m long underactuated feeder vessel to approach a dock. The trajectory can be used by a feedback controller to steer the vessel to the dock, and the time derivatives can be used to construct a feed forward signal to improve the tracking performance.
An optimal control problem is formulated to answer i) what the best pose is to start an approach to the dock, and ii) what trajectory is optimal from an arbitrary initial pose. The resulting trajectory gives an optimal minimal-time solution, but the computational time was too large to employ real-time. A second trajectory was constructed based on Bézier curves. The computational load of this trajectory is negligible. The trajectory can be used for a subset of initial states. It does provide a smooth trajectory with all the derivatives, and is seen as a good option when the vessel starts the docking manoeuvre from a not too challenging pose.

Keywords: Berthing/docking control, Optimal Control Problem, Bézier curves

1. INTRODUCTION

Autonomous sailing is seen as one of the possible solutions to cope with the decrease in qualified officers, to minimise the risk to humans and ships in challenging conditions, and to minimise the environmental impact of the transport sector. Autonomous sailing is not limited to move the vessel safely through oceans, seas and canals, but it also includes automatic docking. To take the full advantage of autonomy and remote operation, even the loading and unloading needs to be done without the intervention of personnel on site. The EU-H2020 Moses project aims at just this: optimise sustainable short sea shipping. A newly designed feeder vessel needs to sail a relative short distance between two quays where it will be automatically unloaded. The vessel has two azimuthing thrusters and two bow thrusters. It is depicted in Fig. 1. This research solely focusses on docking.

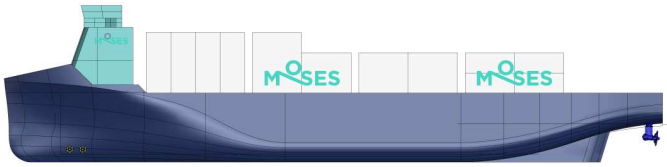

Fig. 1. The feeder vessel used in this study.

The manoeuvre from sailing waypoints to being docked at a quay can be divided into three parts. In the first phase, the transit phase, the ship is tracking a path defined by waypoints at a near constant speed. The next two phases are concerned with the docking procedure (Okazaki and Ohtsu, 2008; Ahmed and Hasegawa, 2015). In the second phase the ship goes to a small, but safe, distance from the actual berthing site with a required heading and negligible speed: termed the approaching phase. During this approaching phase the ship has to decrease its surge velocity to near zero. In this phase our ship can only be controlled with the azimuthing thrusters, and is hence underactuated. In the final phase, the ship is moving very slowly from the end of the approaching phase to the actual dock. Typically the bow thrusters are now used to move the ship (sideways). This can be done either by hand or with a dynamical positioning system. This phase will be indicated as the docking phase.

We divide the problem for each phase into trajectory generation, control design and actuator allocation in order to simplify the individual designs. Within the docking manoeuvre we further reduce the scope to trajectory generation. This step needs to be solved first, as a reference signal is needed for the controller. Furthermore, the trajectory needs to be feasible for our underactuated ship with azimuthing pods that have bounds on how fast they rotate, and how much thrust they can provide. During the approaching phase it is of importance to deviate little from the trajectory, as the space is often confined. Providing the time derivatives of the trajectory enables a feed forward control signal that improves the track following accuracy. The objective of this work is hence to construct a trajectory, including its time derivatives, during the approaching phase that can be provided to a controller to follow. It

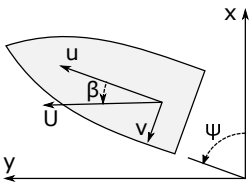

Fig. 2. Variables used in the North-West-Up (NWU) coordinate system.

should connect well with the preceding transit phase and following docking phase.

A common approach to find such a trajectory is to formulate it as an Optimal Control Problem (OCP), which is often encountered in the literature (Djouani and Hamam, 1995; Ohtsu et al., 1996). This OCP calculates a trajectory from the initial state to the final state when it enters the docking phase. The generation thereof is treated in section 5. A trajectory from this initial state will also be generated with a Bézier curve which has much smaller computation requirements. The results of both approaches will be compared.

The approaches found in the, more methodological, literature calculates the trajectory from some distance to the dock. The distance from which the approaching phase is started can be as small as 5 ship lengths (Martinsen et al., 2019) till about 30 ship lengths (Han et al., 2021) and anything in between. The majority starts the approaching phase around 10 ship lengths with an arbitrary heading. However, we influence ourself where and when we start the docking manoeuvre, and what the approximate heading will be at that time. Therefore in section 4 we calculate the optimal approach heading and distance, such that the trajectory from this state to the docking phase becomes as simple as possible. This can be done, again, with an OCP. In order to formulate the OCP we need the system equation of our vessel. Generation of the model will be treated in section 2.

2. MODEL

The model used in our study is based on manoeuvring coefficients, equivalent to (Yasukawa and Yoshimura, 2015):

$$\begin{aligned}(m - X_{\dot{u}})\dot{u} &= mvr + X_{uu}u^2 + X_{uv}uv \\ &\quad + X_{vr}vr + X_{rr}r^2 + \tau_x \\ (m - Y_{\dot{v}})\dot{v} &= -mur + Y_{uv}uv + Y_v v \\ &\quad + Y_{vvv}v^3 + Y_{ur}ur + Y_{rrr}r^3 + \tau_y \\ (I_{zz} - N_{\dot{r}})\dot{r} &= N_{uv}uv + N_v v + N_{vvv}v^3 \\ &\quad + N_r r + N_{rrr}r^3 + N_{ur}ur + \tau_r,\end{aligned} \tag{1}$$

in which τ_i are the forces and moment from the azimuthing pod, as treated next. The ship-fixed surge velocity, sway velocity and rate of turn are denoted by u, v, r. The ships mass is given as m. The other terms are the manoeuvring coefficients, and their (dimensionless) values are provided in table 1. These equations set the origin in the centre of gravity, and ignore the effect of $N_{\dot{v}}, Y_{\dot{r}}$. The coordinate system and variables used are shown in Fig. 2. In this figure, Ψ denotes heading, β the drift angle and U the total speed. The manoeuvring coefficients were fitted to CFD computations of a feeder vessel. The fit was made for small drift angles and yaw-rates. In order for the model to be valid, the following constraints have to be met:

Table 1. Non-dimensional manoeuvring coefficients for (1) in the bis system (Norrbin, 1971).

L	1	X_{uu}	-5.84e-2	Y_{rrr}	-4.72e+1
m	1	X_{uv}	-3.54e-1	N_{uv}	-4.25-1
I_{zz}	6.25e-2	X_{vr}	5.41e-1	N_v	-5.15e-2
$X_{\dot{u}}$	-5.01e-2	Y_{uv}	-4.74e-1	N_{vvv}	-2.94e+1
$Y_{\dot{v}}$	-1.05	Y_v	-3.36e-3	N_r	-1.46e-3
$N_{\dot{r}}$	-8.56e-2	Y_{vvv}	-1.23e-4	N_{rrr}	-4.18e+0
X_{rr}	3.90e-3	Y_{ur}	1.01e-1	N_{ur}	-1.25e-1

$$\beta \leq 10^\circ \rightarrow \frac{v}{u} \leq \frac{U\cos\beta}{U\sin\beta} \approx 0.17, \tag{2}$$

$$r \leq 0.05 (= r_{\max}) \text{ rad/s}, \;\; u \geq 0 \text{ m/s}. \tag{3}$$

In the remainder of the text we will work and report in dimensionless variables.

The vessel is equipped with two azimuthing pods, and two bow thrusters. The bow thrusters are not effective at high surge velocities, and are not used in the trajectory generation. The two azimuthing pods are treated as a single actuator during the approaching phase. They are modelled as a single rotatable force actuator. The conversion from thrust F to RPM will be addressed by the allocation algorithm. The maximum thrust of the combined pods is 500 kN and can only be positive. They spin up or down in ten seconds, and the azimuth angle can change with a maximum speed of 5 degrees per second. The constraints of the dimensionless actuator, converted with (Norrbin, 1971), then become:

$$\begin{aligned} 0 \leq & F \leq 0.0121, \\ -3.5 \cdot 10^{-3} \leq & \dot{F} \leq 3.5 \cdot 10^{-3}, \\ -0.25 \leq & \dot{\alpha} \leq 0.25 (= \dot{\alpha}_{\max}), \end{aligned} \tag{4}$$

with α the azimuthing angle. The pods are located at the stern, and with the centre of gravity set in the middle, the actuator forces become:

$$\tau_x = F\cos(\alpha), \quad \tau_y = F\sin(\alpha), \quad \tau_r = 0.5F\sin(\alpha).$$

The factor 0.5 in the last term indicates the normalised arm on which the thrust acts.

3. OPTIMAL CONTROL PROBLEM

The optimisation of a trajectory to go from an initial state to a final state can be solved by means of an Optimal Control Problem (Kirk, 2004). Our OCP minimises:

$$\min_{t_f, \dot{F}, \dot{\alpha}} \; t_f + (x(t_f) - x_f)^T Q (x(t_f) - x_f), \tag{5}$$

in which t_f is the final time and the state is $x = [N, W, \psi, u, v, r, F, \alpha]$. The change in thrust and change in azimuthing angle, as well as the final time are the independent variables. The actual thrust and azimuthing angle are part of the state. The matrix Q weighs the difference between the realised and required final state. It contains large values on its diagonal, except for the final azimuthing angle. This type of optimisation is known as a minimal time optimisation. It is also used by (Ohtsu et al., 1996; Okazaki and Ohtsu, 2008; Mizuno et al., 2015).

In our runs the required final state components are all zero, except the required final heading, which is given as a 20° degrees deviation parallel to the dock. This approach

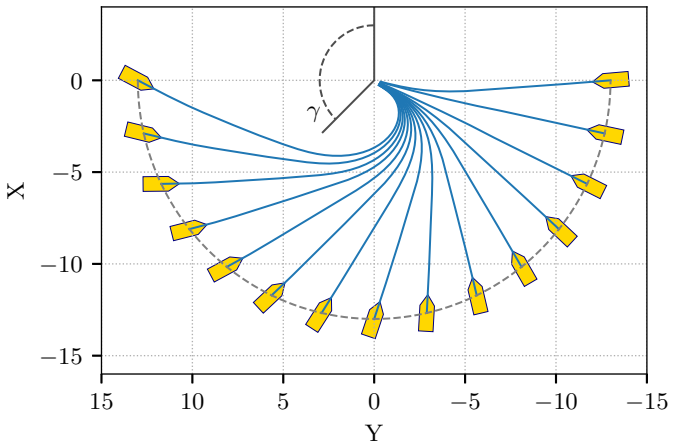

Fig. 3. Time optimal trajectory for different start positions. The initial velocity and heading are calculated.

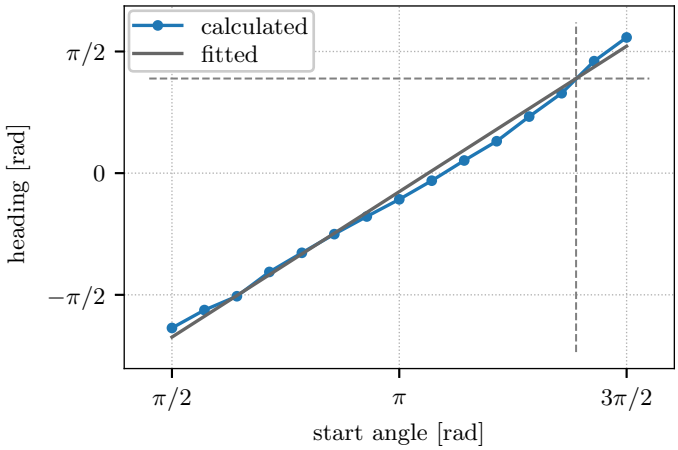

Fig. 4. The optimal initial heading as function of the start angle to the dock.

is also used, although implemented completely different, in (Ahmed and Hasegawa, 2015). In the last stretch of the approach the vessel should sail straight and only decelerate. A small offset angle is used to have a safety margin to the dock as not to collide with the dock due to suction, or environmental disturbances. The system dynamics (1), the model validity range (2), (3), and the actuator limits (4) are used to constraint the solution of the OCP. To get a smooth transition to the docking phase, the thrust is constraint close to the docking position as:

$$|F| \leq F_{\max}/10 \cdot D, \tag{6}$$

with D the distance to the docking point. Due to this constraint, there is no thrust at the end of the approaching phase and we can transition smoothly to the docking phase.

The OCP is implemented with the help of CasADI (Andersson et al., 2019). A direct collocation approach is used based on one of their examples. The time horizon was discretised into 100 segments, and on each segment the derivatives of the system dynamics were fitted with second order Legendre polynomials. Higher order polynomials or the use of more segments did not influence the solution obtained.

4. TRANSITION TO APPROACHING PHASE

The first question that needs to be answered is from which distance and heading we want to transition from the transit phase to approaching the dock. The OCP that was introduced in the previous section can be used to determine this. If we specify the initial position at different distances, but leave the initial heading and surge velocity free, then the OCP will calculate the optimal track to the final state, in combination with the optimal initial velocity and initial heading. The sway velocity, rate of turn and the azimuthing angle are set to zero to indicate that we start by sailing straight. This tells how we should select the last waypoint before we transition to the docking manoeuvre for the different distances to the dock. Fig. 3 shows the optimal trajectory and initial heading for different start angles γ to the dock. For all these initial poses the resulting optimal starting velocity was the maximum ship velocity. The distance to the dock in this figure is 13 ship lengths.

The same calculation has been done for a multitude of distances, although not shown here. If the initial distance to the berthing location would be set larger, then the solution steers the vessel straight at maximum velocity until it reaches this distance. It is therefore of no use from the OCP point of view, to start at a distance larger than 13 ship lengths. *If* the distance dependent constraint on the thrust (eq. 6) was *not* used, then this distance could be decreased to nine ship lengths. Note that going from maximum speed, which would be 24kn, to standstill in nine ship lengths is possible from the model calculations, but would be exciting, and a safety margin on the speed is recommended from a practical point of view.

If a smaller distance to dock is selected to transition with zero rate-of-turn, then a solution might still be obtained. From that state it will of course be the time minimal solution. However, the time from this initial condition *plus* the time to get to it from the 13 ship lengths distance, is larger than the time needed if the approaching phase was started at 13 ship lengths. At too small distances, the solution becomes infeasible.

Fig. 4 shows the optimal initial heading as function of the start angle. A start angle $\gamma = \pi$ radians indicates that it start south of the dock. The dotted horizontal and vertical lines show the situation where the vessel starts in the correct direction to dock and only needs to decelerate to reach the final desired state. The blue line with dots show the optimal calculated headings. The optimal initial heading is approximated linearly as shown by the black line:

$$\psi_0 = 1.20(\gamma - \psi_\mathrm{f} - \pi) + \psi_\mathrm{f}. \tag{7}$$

In practice the vessel can deviate from the optimal initial heading due to disturbances. In the next section the trajectory for any *given* initial state is calculated.

5. APPROACHING PHASE

In order to calculate the trajectory from a given state, we constrain the initial state of the OCP to these values. The only difference with the previous section is that the initial heading and surge velocity are no longer independent variables. As we do not want the ship to increase its surge velocity during the approach, the constraint $u(t) \leq$

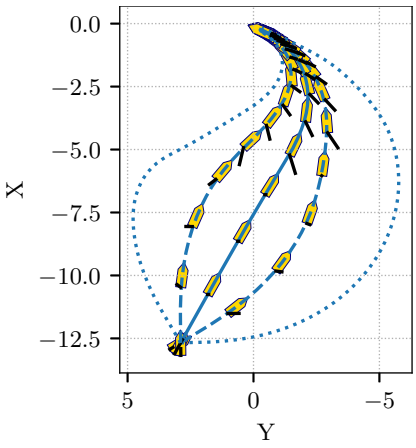

(a) Trajectory

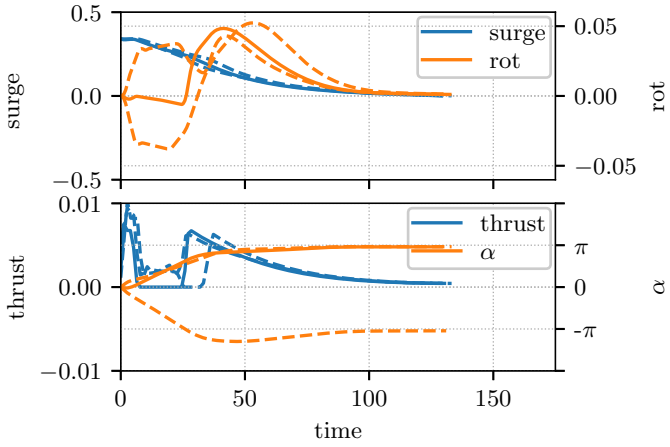

(b) Time traces, all variables are dimensionless

Fig. 5. Trajectory and selected time traces when entering the approaching phase at different headings. Surge velocity is $u = 2/3u_{\max}$

$u(0)$ is added. Actuator usage is slightly penalised in the presented results for numerical stability.

A typical trajectory is shown in Fig. 5. Fig. 5(a) shows the path that the vessel takes when it starts at the optimal initial heading, and for deviations of $\pm 30°$ and $\pm 60°$ thereof. The black line at the back of the vessel shows the force vector of the azimuthing thruster. Fig. 5(b) shows time traces for these trajectories. The solid line depicts the line for the optimal initial heading, while the dashed lines show it for a deviation of $\pm 30°$ degrees. The blue lines correspond to the left-hand side y-axis for surge and thrust, and the orange lines with the right-hand side y-axis for rate of turn and azimuthing angle.

The result are as expected. In all cases the surge speed reaches zero at the end. When the vessel is at the optimal initial heading, the rate of turn is zero for the initial part. When there is a deviation of the optimal heading, then the vessel needs to turn at the beginning of the run. Although the differences are small, the time is shortest with the optimal heading. The constraints that were set in the OCP are obviously met with these solutions. The calculations took between one second and one minute on a laptop with Intel i7-8650U CPU and makes it difficult to use it directly in the control loop, even if it only needs to be computed at the beginning of the approaching phase. The computation time has been resolved in literature by computing a large set of initial conditions, and use a neural net to interpolate between these (Okazaki and Ohtsu, 2008; Ahmed and Hasegawa, 2015). This has shown good results, however, it is not employed in this study as it is not transparent what is exactly learnt, nor does the learnt solution provide information on the derivatives. In order to deal with the computational time, a Bézier curve is used to describe the path (Djouani and Hamam, 1995; Sawada et al., 2021). Such a curve does not contain any model information and it cannot guarantee that the limitations on, i. e., rate of turn are met beforehand. Hence, the approach with parametric curves is not as versatile as an OCP.

5.1 Bézier trajectory

A Bézier curve is a parametrised curve in space (Kamermans, 2022). As such, it can be used to smoothly connect two points in space. Refer to appendix A for derivations used in this section. The equation for a cubic Bézier curve is given as:

$$B(s) = (1-s)^3 p_0 + 3(1-s)^2 s p_1 + 3(1-s)s^2 p_2 + s^3 p_3. \quad (8)$$

Fig. A.1 illustrates the variables used in this equation. The curve variable s indicates where we are on the curve. The trajectory is defined by selecting the control points and the function relating time s.

The initial and final position define the values for control points p_0 and p_3. The tangent at p_0 is equal to the vector from p_0 to p_1. The length of this vector is set to $l_0 = 0.6D$, which closely matches (Sawada et al., 2021), and fully specifies p_1. D is again the distance to the dock. The value for p_2 is set such that the vector from it to p_3 equals the final heading. The length of this vector is set to 5 ship lengths, $l_f = 5$, again from (Sawada et al., 2021). The control points fully specify the path in space, but it should also be specified how the path is traversed. This is defined by how the curve variable s depends on time. We select it as the polynomial: $s(t) = t/T(2 - t/T)$. This function guarantees that the final velocity is zero, see appendix A. The duration of the run is fully related to the length l_0 and the initial velocity by $T = 6l_0/u_0$. The speed, heading and their time derivatives are given in the appendix for each time step. Note that the constraints cannot be explicitly incorporated, and must be tested after the generation of the trajectory.

We compare the resulting Bézier trajectories with the OCP solution. The trajectories were calculated for the optimal heading, the optimal heading $\pm 30°$, and $\pm 60°$ degrees, and for an initial velocity $u(0) = 0.5u_{\max}$, $u(0) = 0.75u_{\max}$ and $u(0) = u_{\max}$. This is done for a set of 15 approach angles. The result of these calculations are shown in Fig. 6. The wedges show whether or not a trajectory is considered valid in green, or invalid in red. A trajectory is classified as valid if both the rate of turn and the acceleration stayed within their bounds, e.g. (3) for the rate-of-turn, and the acceleration calculated from the maximum thrust and the mass (4). The direction of the wedge shows the initial heading, and the length of the wedge shows the initial velocity. If, for example, only the outer part of a wedge is red, then this indicates that the generated trajectory is only invalid for maximum velocity. In addition to the

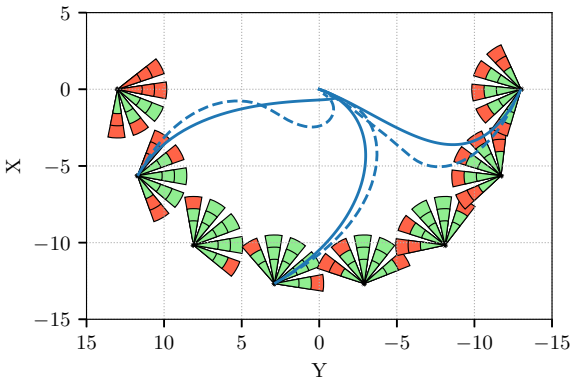

Fig. 6. Start conditions in which the Bézier curve gives a valid trajectory. The solid lines are the Bézier curves, and the dashed lines result from the OCP.

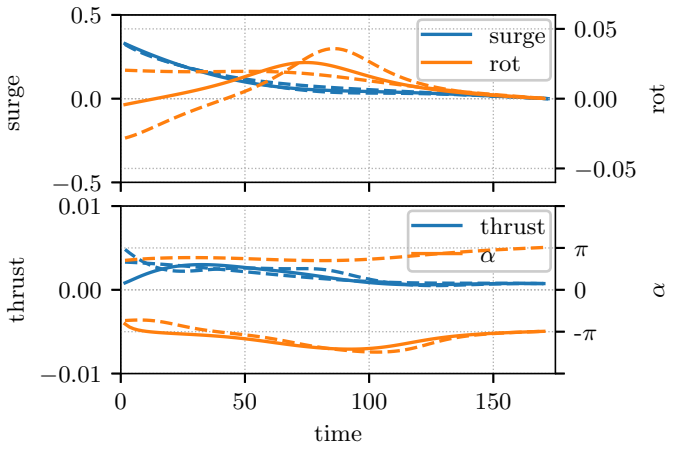

Fig. 7. Time trace for the Bézier curve trajectory. The solid line is the optimal initial heading, the dashed lines represent the ±30° deviations.

validity of a trajectory, several of these trajectories are shown. The dashed lines show the OCP solution, and the solid lines show the Bézier trajectory.

The time traces corresponding to the initial state used in Fig. 5 are shown in Fig. 7. The corresponding path is also shown starting from $x = -12.7, y = 2.9$ in Fig. 6. Fig. 6 shows that the trajectory generated from a Bézier curve stays often within the limits for acceleration and rate of turn. This holds especially if the initial velocity is not set to its maximum. And the initial heading should not be opposite to the final heading, with all the control points nearly laying on a line. The first would require a fast drop in velocity which the thrusters cannot generate. The letter requires a high curvature at the end of the path, as shown in the left path of Fig. 6.

Comparison of the time traces of the OCP and the Bézier trajectory shows some interesting results: the duration needed to reach the docking phase is shorter for the OCP: 131 versus 171. As the time is explicitly minimised for the OCP, this is as expected. The median of this ratio for all the valid Bézier trajectories is found to be 1.36. Furthermore, the Bézier trajectory start with a non-zero rate of turn. In the OCP the azimuthing thrusters had to start from a zero angle, so the vessel could not start rotating directly. An initial zero rate of turn can be achieved by increasing the order of the Bézier curve. The median on the ratio of the maximum rate of turn between OCP and Bézier trajectories is 0.66. This is as expected, as the duration of the approaching phase takes longer with the Bézier trajectory. However, there are initial states for which the maximum rate-of-turn is much larger than for the OCP trajectory: nearly a factor two. It is therefore important to check the validity of the Bézier curve before using it. The path of the Bézier curve is fully specified by the control points. These do not change based on the initial velocity, and hence the path is the same for all velocities. The OCP does change its path based on the initial velocity. If the initial velocity is larger, then its curvature will be lower at the beginning of the run such that the rate of turn stays within its limits.

The computational time of the Bézier trajectory is negligible in comparison with the OCP: it took approximately 0.2 ms to evaluate the trajectory at 100 points on a laptop with Intel i7-8650U CPU core. An additional advantage is an analytic relation is available for all positions, velocities and accelerations, with which we can calculate the values at any time instance we require. There is no need to do interpolation in the discretised solution of the OCP.

6. CONCLUSIONS

The aim of this study was to construct a trajectory, including its time derivatives, to approach a dock for our underactuated feeder vessel. Two approaches were employed to reach the dock. First an Optimal Control Problem was formulated to go from any initial state to the dock in minimum time. The trajectories resulted in tracks that the vessel could track and which would uphold the given constraints. A model of the vessel was needed to guarantee this. The computation time of such an algorithm too large to run at real-time.

As simple and fast alternative, a trajectory based on a Bézier curve is introduced. The computational time is negligible and can easily be done in real-time. It resulted in a smooth trajectory that can be evaluated at any arbitrary time. However, the approach is based on kinematics, and not on the actual dynamics of our vessel. The limits on the velocities and acceleration are not guaranteed beforehand, and must be checked afterwards. Even if the velocity and acceleration is within their bounds, the *underactuated* vessel might still not be able to track it perfectly. This might not pose a problem, as environmental disturbances and model uncertainty always require a feedback controller to follow a trajectory specified. The OCP has also been used to find when and how our vessel should transition from sailing a track specified by waypoints to approaching the dock. This resulted in an optimal heading to start the approaching phase to make the docking as simple as possible. The next step is to compare the two trajectories in a controlled system and test the difference in performance.

Acknowledgment MOSES project has received funding from the European Union's Horizon 2020 research & innovation programme under grant agreement No. 861678. Content reflects only the authors' view and the Agency is not responsible for any use that may be made of the information it contains.

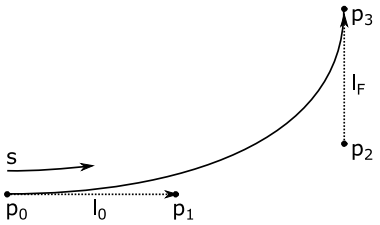

Fig. A.1. The principle variables of a cubic Bezier curve.

Appendix A. BÉZIER CURVE

A cubic Bezier curves are defined as (Kamermans, 2022):

$$B(s) = (1-s)^3 p_0 + 3(1-s)^2 s p_1 + 3(1-s)s^2 p_2 + s^3 p_3.$$

With $0 \leq s \leq 1$. The variables used are shown in Fig. A.1. B and p_i are 2×1 vectors that contain the values for x and y respectively. When we set $s = 0$ then this function evaluates to p_0, and at $s = 1$ we get p_3. The derivative with respect to s is calculated as:

$$B'(s) = 3(1-s)^2(p_1-p_0)+6(1-s)s(p_2-p_1)+3s^2(p_3-p_2)$$

At $s = 0$ and $s = 1$ this evaluates to $B'(0) = 3(p_1 - p_0)$ and $B'(0) = 3(p_3 - p_2)$. So, the tangent at the start and the end are given by the vector to the adjacent control point. If we want to know the desired position, velocity and acceleration, then we have to define a function that maps time t to the curve variable s. If this function is known, we can calculate the surge velocity as:

$$u(t) = \sqrt{\left(\frac{\mathrm{d}x}{\mathrm{d}t}\right)^2 + \left(\frac{\mathrm{d}y}{\mathrm{d}t}\right)^2} = \frac{\mathrm{d}s}{\mathrm{d}t}\sqrt{\left(\frac{\mathrm{d}x}{\mathrm{d}s}\right)^2 + \left(\frac{\mathrm{d}y}{\mathrm{d}s}\right)^2}. \tag{A.1}$$

Note that the surge velocity is *defined* to be positive! The acceleration in surge direction can be found as:

$$\frac{\mathrm{d}u(t)}{\mathrm{d}t} = \frac{\mathrm{d}}{\mathrm{d}t}\sqrt{\left(\frac{\mathrm{d}x}{\mathrm{d}t}\right)^2 + \left(\frac{\mathrm{d}y}{\mathrm{d}t}\right)^2} = \frac{\frac{\mathrm{d}x}{\mathrm{d}t}\frac{\mathrm{d}^2x}{\mathrm{d}t^2} + \frac{\mathrm{d}y}{\mathrm{d}t}\frac{\mathrm{d}^2y}{\mathrm{d}t^2}}{u(t)}.$$

The higher order chain rule can be used to calculate $\frac{\mathrm{d}^2x}{\mathrm{d}t^2}$. The heading along this curve and its derivatives are calculated as:

$$\begin{aligned}
\psi &= \arctan 2(\mathrm{d}y/\,\mathrm{d}s, \mathrm{d}x/\,\mathrm{d}s),\\
\frac{\mathrm{d}\psi}{\mathrm{d}t} &= \left(\frac{\mathrm{d}^2y}{\mathrm{d}t^2}\frac{\mathrm{d}x}{\mathrm{d}t} - \frac{\mathrm{d}y}{\mathrm{d}t}\frac{\mathrm{d}^2x}{\mathrm{d}t^2}\right) \Big/ u^2(t),\\
\frac{\mathrm{d}^2\psi}{\mathrm{d}t^2} &= (n_1 + n_2 + n_3)\,/u^4(t), \quad \text{with}\\
n_1 &= -2\left(\frac{\mathrm{d}x}{\mathrm{d}t}\frac{\mathrm{d}^2x}{\mathrm{d}t^2} + \frac{\mathrm{d}y}{\mathrm{d}t}\frac{\mathrm{d}^2y}{\mathrm{d}t^2}\right)\frac{\mathrm{d}x}{\mathrm{d}t}\frac{\mathrm{d}^2y}{\mathrm{d}t^2},\\
n_2 &= +2\left(\frac{\mathrm{d}x}{\mathrm{d}t}\frac{\mathrm{d}^2x}{\mathrm{d}t^2} + \frac{\mathrm{d}y}{\mathrm{d}t}\frac{\mathrm{d}^2y}{\mathrm{d}t^2}\right)\frac{\mathrm{d}y}{\mathrm{d}t}\frac{\mathrm{d}^2x}{\mathrm{d}t^2},\\
n_3 &= -\left(\frac{\mathrm{d}y}{\mathrm{d}t}\frac{\mathrm{d}^3x}{\mathrm{d}t^3} - \frac{\mathrm{d}x}{\mathrm{d}t}\frac{\mathrm{d}^3y}{\mathrm{d}t^3}\right)\left(\left(\frac{\mathrm{d}x}{\mathrm{d}t}\right)^2 + \left(\frac{\mathrm{d}y}{\mathrm{d}t}\right)^2\right).
\end{aligned}$$

A mapping is needed from time to the curve variable s. This mapping needs to be monotonously increasing. Eq. (A.1) has to hold for the boundary conditions. Evaluating the derivative of the cubic Bézier curve at $s = 0$ and $s = 1$ results in

$$u_0 = 3l_0\frac{\mathrm{d}s(0)}{\mathrm{d}t}, \quad u_\mathrm{f} = 3l_\mathrm{f}\frac{\mathrm{d}s(1)}{\mathrm{d}t}$$

As we want to end at zero speed, $u_\mathrm{f} = 0$ and we want to have l_f finite, we need $\frac{\mathrm{d}s(1)}{\mathrm{d}t} = 0$. The polynomial $s(t) = t/T(2 - t/T)$, among many others, fulfils this. The derivative at $t = 0$ evaluates to $\frac{\mathrm{d}s(0)}{\mathrm{d}t} = 2/T$. This can be related to the initial velocity:

$$u_0 = \frac{6l_0}{T}. \tag{A.2}$$

From which the duration can be calculated.

REFERENCES

Ahmed, Y. and Hasegawa, K. (2015). Consistently Trained Artificial Neural Network for Automatic Ship Berthing Control. *TransNav, the International Journal on Marine Navigation and Safety of Sea Transportation*, 9(3), 417–426.

Andersson, J.A., Gillis, J., Horn, G., Rawlings, J.B., and Diehl, M. (2019). CasADi: a software framework for nonlinear optimization and optimal control. *Mathematical Programming Computation*.

Djouani, K. and Hamam, Y. (1995). Minimum Time-Energy Trajectory Planning for Automatic Ship Berthing. *IEEE Journal of Oceanic Engineering*, 20(1), 4–12.

Han, S., Wang, Y., Wang, L., and He, H. (2021). Automatic berthing for an underactuated unmanned surface vehicle: A real-time motion planning approach. *Ocean Engineering*, 235(January), 109352.

Kamermans, M. (2022). A Primer on Bézier Curves.

Kirk, D.E. (2004). *Optimal Control Theory, An Introduction*. Dover Publications, Mineola, New York.

Martinsen, A.B., Lekkas, A.M., and Gros, S. (2019). Autonomous docking using direct optimal control. *IFAC-PapersOnLine*, 52(21), 97–102.

Mizuno, N., Uchida, Y., and Okazaki, T. (2015). Quasi Real-Time Optimal Control Scheme for Automatic Berthing. *IFAC-PapersOnLine*, 48(16), 305–312.

Norrbin, N.H. (1971). Theory and observations on the use of a mathematical model for ship manoeuvring in deep and confined waters. Technical Report August 1970, Statens Skeppsprovningsanstalt, Goteborg.

Ohtsu, K., Shoji, K., and Okazaki, T. (1996). Minimum-time maneuvering of a ship, with wind disturbances. *Control Engineering Practice*, 4(3), 385–392.

Okazaki, T. and Ohtsu, K. (2008). A study on ship berthing support system - Minimum time berthing control -. In *2008 IEEE International Conference on Systems, Man and Cybernetics*, 1522–1527. IEEE.

Sawada, R., Hirata, K., Kitagawa, Y., Saito, E., Ueno, M., Tanizawa, K., and Fukuto, J. (2021). Path following algorithm application to automatic berthing control. *Journal of Marine Science and Technology*, 26(2), 541–554.

Yasukawa, H. and Yoshimura, Y. (2015). Introduction of MMG standard method for ship maneuvering predictions. *Journal of Marine Science and Technology*, 20(1), 37–52.